

Magnetic proximity effects in antiferromagnetic composite thin films: Roles of triggering perpendicular magnetic anisotropy

Bo-Yao Wang ^{1,*}, Tzu-Hsin Li,¹ Bo-Xiang Liao,¹ Chung-Hsuan Hsiao ¹, Li-Han Chang,^{1,2} Ming-Shian Tsai,^{1,2}
Tzu-Hung Chuang,³ and Der-Hsin Wei ³

¹*Department of Physics, National Changhua University of Education, Changhua 500, Taiwan*

²*Institute of Photonics Technologies, National Tsing Hua University, Hsinchu 300, Taiwan*

³*National Synchrotron Radiation Research Center, Hsinchu 300, Taiwan*



(Received 21 August 2023; revised 27 October 2023; accepted 31 October 2023; published 14 November 2023)

Antiferromagnetic (AFM) thin films have been proposed as a promising material for manipulating perpendicular magnetic anisotropy (PMA) in ferromagnetic (FM) thin films. In this work, a series of epitaxially grown AFM/Co/Fe structures are investigated, in which the AFM layer is composed of fcc Fe₅₀Mn₅₀ and vertically expanded face-centered-tetragonal Mn films with distinct three-dimensional quadratic-type and two-dimensional layered spin structures, respectively. Our findings demonstrate that an individual AFM film in the composite AFM layer not only can enhance the long-range AFM ordering in its adjacent AFM neighbor but also can exert control over the neighbor's AFM spin structure; these modulation mechanisms subsequently induce PMA in an adjacent FM film. The research sheds light on the AFM proximity effects within the AFM composite layers and their profound influence on PMA induction in adjacent FM layers, offering essential insights for improving control over PMA with AFM layers.

DOI: [10.1103/PhysRevB.108.184412](https://doi.org/10.1103/PhysRevB.108.184412)

I. INTRODUCTION

Antiferromagnetic (AFM) thin films, with their local spin moments and diverse AFM structures, have garnered much research interest due to their valuable physics and practical applications. The combination of AFM and ferromagnetic (FM) layers results in the phenomena of coercivity (H_c) enhancement and exchange bias [1–4], which are crucial for stabilizing the magnetic reference layer in contemporary magnetic devices [5]. Recently, AFM thin films have been proposed as promising materials for inducing magnetic anisotropy on FM films [6–10]. In particular, the ability to trigger perpendicular magnetic anisotropy (PMA) in adjacent FM films [11–19] is crucial for the potential application of state-of-the-art perpendicularly based spintronic devices. The strength of AFM-induced PMA in FM films is influenced by the AFM film thickness and spin structure, as well as finite-size effects on AFM/FM exchange coupling [20]. Due to the higher energy scale of exchange coupling [21], the PMA induction approach using AFM layers could potentially provide more control over PMA strength in FM films compared to conventional mechanisms through orbital hybridization and spin-orbit coupling [22–25].

fcc Fe₅₀Mn₅₀ has received particular attention among AFM materials due to its unique three-dimensional quadratic-type (3Q) spin structure that exhibits uncompensated spin components in the out-of-plane direction [Fig. 1(a)] [26–29]. Previous studies have indicated that fcc Fe₅₀Mn₅₀ films, when reaching an AFM state at approximately 9 monolayers

(ML), can induce high-strength PMA in adjacent Co/Fe films through collinearlike exchange coupling at room temperature [16,30]. However, under the same thickness conditions, the vertically extended face-centered-tetragonal (e-fct) Mn film, characterized by a higher AFM ordering temperature [31–35] but with a two-dimensional layered spin structure [Fig. 1(b)] [36,37], exhibits much weaker induced PMA strength. High-strength PMA in the e-fct Mn/Co/Fe film can be triggered only below 190 K through a noncollinear exchange coupling resulting from the interplay of exchange and spin-orbit coupling across the AFM-FM interface [15,17,30]. With a single AFM layer, it is difficult to simultaneously achieve high AFM ordering temperatures and suitable AFM spin structure for the PMA induction. As a result, applying AFM composite films could be a potential solution for better PMA induction conditions. Using heterospin structures in AFM composite films has been suggested to modulate the AFM ordering temperature through “AFM proximity effects” [38]. However, the AFM proximity effects within the AFM films for the PMA induction of adjacent FM layers have yet to be studied.

In this paper, we report the effects of triggering PMA in a 3-ML Co/3-ML Fe/Cu(001) (Co/Fe/Cu) film by applying composite AFM layers composed of fcc Fe₅₀Mn₅₀ and e-fct Mn films with 3Q-type [Fig. 1(a)] and two-dimensional layered AFM spin structures [Fig. 1(b)] [26–29,36,37], respectively. Our results demonstrate that one AFM film can promote long-range AFM ordering and even modulate the AFM spin structure of the adjacent AFM film. This modulation mechanism in the composite AFM layers subsequently induces PMA in an adjacent FM film. Our finding clarifies the AFM proximity effects within the AFM composite layers and highlights its impact on PMA induction of the

*bywang1735@cc.ncue.edu.tw

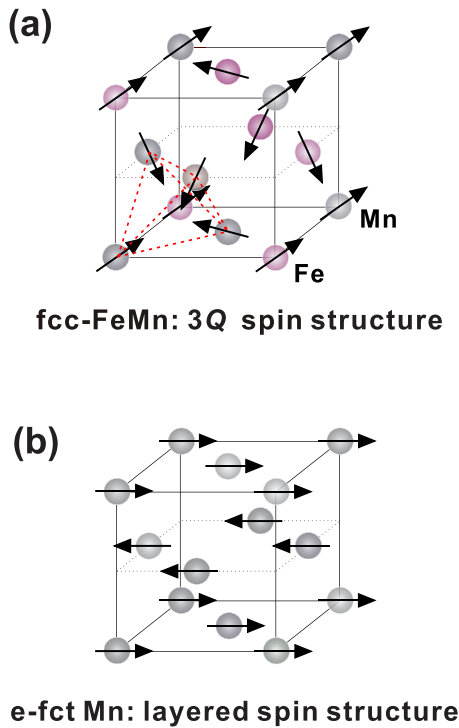


FIG. 1. (a) and (b) Schematic illustrations of the three-dimensional quadratic-type (3Q-type) and layered-AFM spin structures of the fcc $\text{Fe}_{50}\text{Mn}_{50}$ and e-fct Mn films, respectively, based on the literature [26–29,36,37].

adjacent FM layers, providing a flexible means of controlling antiferromagnet-induced PMA.

II. EXPERIMENT

This study investigates the growth conditions, crystalline structure, and magnetic properties of a series of Mn/Fe₅₀Mn₅₀/Co/Fe/Cu and Fe₅₀Mn₅₀/Mn/Co/Fe/Cu layers *in situ* within a multifunctional ultrahigh-vacuum chamber with a base pressure of 2×10^{-10} Torr. Cu(001) single-crystal substrates with miscut angles less than 0.1° were cleaned by cycles of 2-keV Ar⁺ ion sputtering followed by annealing at 800 K for 5 min to attain a well-ordered crystalline structure and a smooth surface. The films were deposited onto Cu(001) at room temperature using electron beam evaporators. Three electron beam evaporators were used to deposit the Fe, Co, and Mn elements, with rod-shaped sources used for Fe, Co, and Mn placed in Mo crucibles. The deposition rate and thickness of the films during growth were monitored using medium-energy electron diffraction (MEED). Figure 2 shows a series of typical specular MEED (0,0) beam intensities of Fe films grown on Cu(001); Co films grown on 3-ML Fe/Cu(001); Mn films grown on 0-, 2-, and 4-ML Fe₅₀Mn₅₀/Co/Fe/Cu; and Fe₅₀Mn₅₀ films grown on 0-, 2-, and 4-ML Mn/Co/Fe/Cu. The regular oscillation indicates layer-by-layer growth conditions for these films. The in-plane and vertical interlayer distances of the films were determined *in situ* using low-energy electron diffraction (LEED) with a kinematic approximation (LEED I/V), as reported in Ref. [39]. The magnetic hysteresis loops of the films were

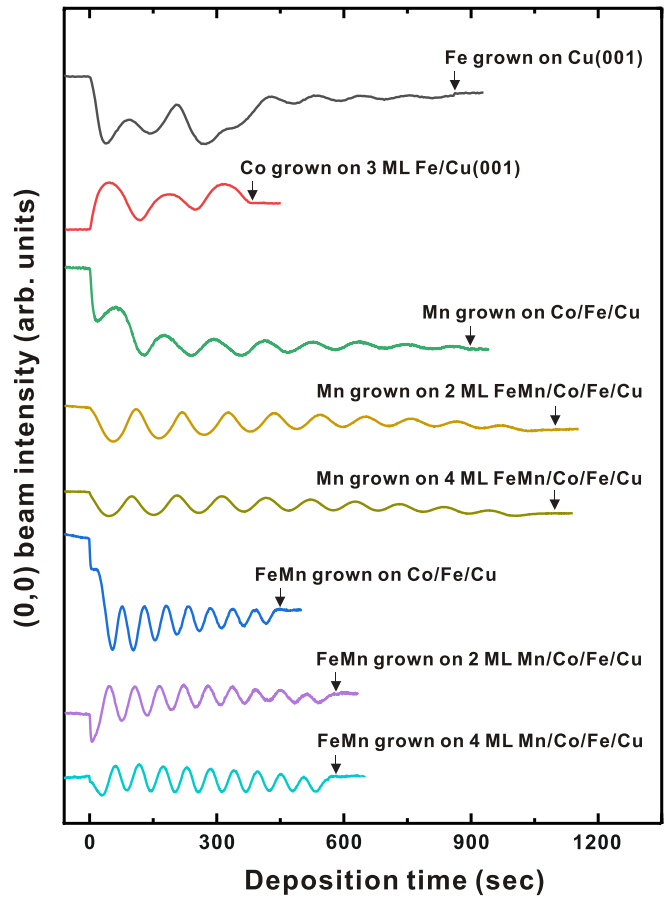


FIG. 2. Selected MEED (0,0) beam intensity curves as a function of deposition time for the Fe film grown on Cu(001), Co film grown on 3-ML Fe/Cu(001), Mn grown on 0-, 2-, and 4-ML Fe₅₀Mn₅₀/Co/Fe/Cu, and Fe₅₀Mn₅₀ grown on 0-, 2-, and 4-ML Mn/Co/Fe/Cu at 300 K. The film thickness was determined from the oscillations in the MEED curves. The arrows indicate the moment the shutter was closed.

measured *in situ* using the longitudinal and polar magneto-optical Kerr effect (MOKE) at temperatures of 300 K. The magnetic field was aligned parallel to the film surface in the longitudinal mode, and it was perpendicular in the polar mode. Both longitudinal and polar MOKEs utilized a 45° angle between the laser beam and the sample, and the measurement signals were obtained with the help of a photomodulator and lock-in technique. The interface magnetic coupling of elements in the PMA-established Fe₅₀Mn₅₀/Mn/Co/Fe/Cu and Mn/Fe₅₀Mn₅₀/Co/Fe/Cu films was detected *in situ* through x-ray magnetic circular dichroism (XMCD) effects [21] at the Co, Fe, and Mn $L_{3,2}$ absorption edges using the total electron yield mode. These measurements were conducted in an x-ray photoemission electron microscopy (PEEM) [40–42] end station at beamline BL05B2 of the Taiwan Light Source at the National Synchrotron Radiation Research Center. The x-ray absorption spectrum (XAS) and XMCD measurements were performed under remanent conditions, created by applying either a positive or negative external magnetic field (± 1000 Oe) along the out-of-plane direction of the samples before they were placed in the fully magnetically shielded sample holder of PEEM.

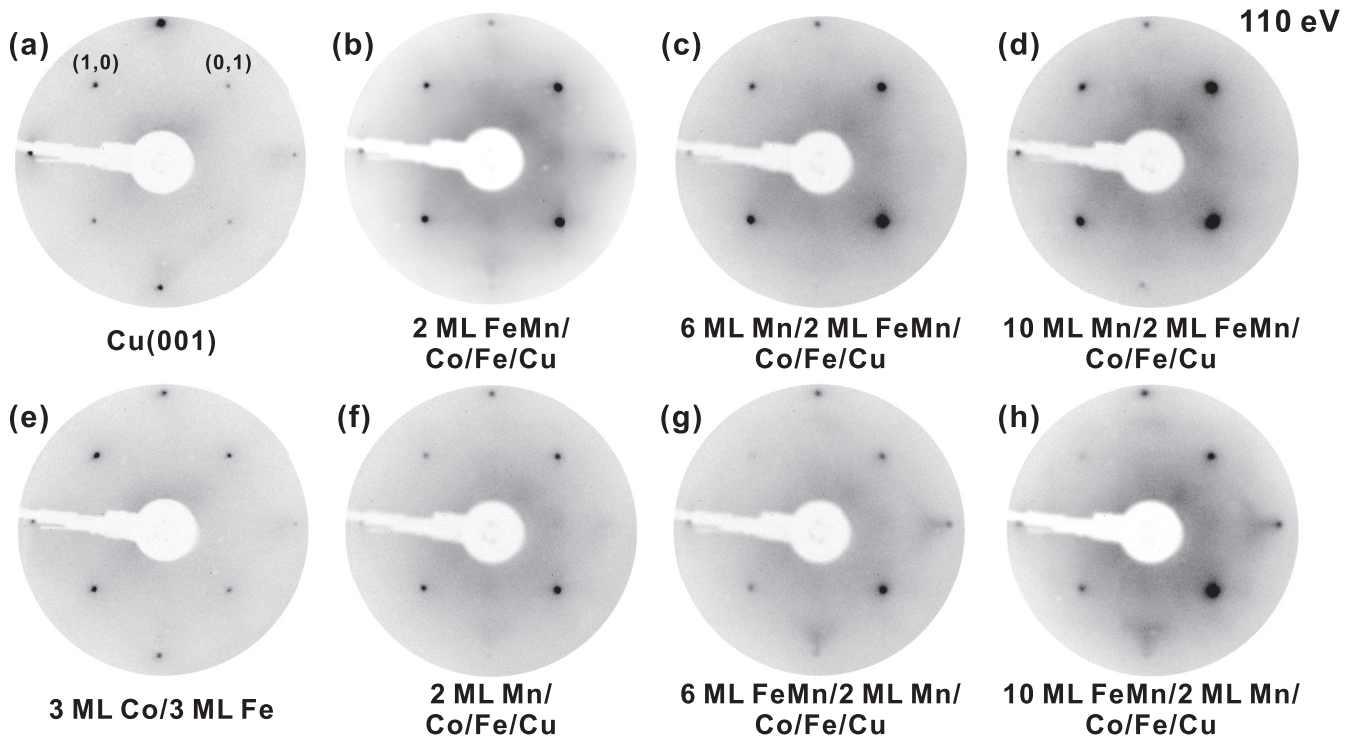


FIG. 3. LEED patterns of (a) Cu(001), (b)–(d) 0-, 6-, and 10-ML Mn/2-ML Fe₅₀Mn₅₀/Co/Fe/Cu, (e) 3-ML Co/3-ML Fe/Cu(001), and (f)–(h) 0-, 6-, and 10-ML Fe₅₀Mn₅₀/2-ML Mn/Co/Fe/Cu, measured at 110 eV and 300 K.

III. RESULTS

A. Crystalline structure of Mn/Fe₅₀Mn₅₀ and Fe₅₀Mn₅₀/Mn grown on Co/Fe/Cu

Figures 3(a)–3(h) show selected LEED patterns of the Cu(001) substrate; 0-, 6-, and 10-ML Mn films grown on 2-ML Fe₅₀Mn₅₀/Co/Fe/Cu; and 0-, 6-, and 10-ML Fe₅₀Mn₅₀ grown on 2-ML Mn/Co/Fe/Cu, respectively. The LEED patterns were captured at 110 eV in 300 K. We found that the $p(1 \times 1)$ spots of the grown films are in the same positions as those of Cu(001), indicating the epitaxial growth condition of the grown films. Thus, the in-plane lattice constants a_{\parallel} of Mn/Fe₅₀Mn₅₀, Fe₅₀Mn₅₀/Mn, and Co/Fe/Cu films were found to be 3.61 Å [the lattice constant of Cu(001)]. No additional LEED spots were observed for Fe₅₀Mn₅₀ films grown on Mn/Co/Fe/Cu, suggesting the Fe₅₀Mn₅₀ layers were chemically disordered crystalline films, in line with previous studies [28,43,44].

Figure 4(a) displays the average interlayer distance d_{\perp} values for 4–12-ML Mn films grown on 0–6-ML Fe₅₀Mn₅₀/Co/Fe/Cu, as calculated from LEED I/V curves similar to Fig. 4(d). When the Mn film thickness exceeds 4 ML, the d_{\perp} value stabilizes at approximately 1.88 Å, revealing an e-fct structure ($c/a \approx 1.04$) of the Mn film. In addition, Fig. 4(b) shows the d_{\perp} value for 4–12-ML Fe₅₀Mn₅₀ films grown on 0–6-ML Mn/Co/Fe/Cu, as calculated from LEED I/V curves similar to Fig. 4(e). The d_{\perp} values of all Fe₅₀Mn₅₀ films were close to 1.81 Å, indicating the formation of an fcc phase of these Fe₅₀Mn₅₀ films. Moreover, Figs. 4(c), 4(f), and 4(g) show that the d_{\perp} values of the topmost 10-ML Mn or 10-ML Fe₅₀Mn₅₀ films are independent of the thickness of the underlying spacer layer (t_{FeMn} or t_{Mn}), further indicating a

coherent growth structure of the e-fct Mn and fcc Fe₅₀Mn₅₀ films on Co/Fe/Cu.

B. Magnetic properties of Fe₅₀Mn₅₀/Co/Fe/Cu and Mn/Co/Fe/Cu

As a model system for the antiferromagnet-induced PMA, the magnetic hysteresis loops of Fe₅₀Mn₅₀/Co/Fe/Cu with a variation of t_{FeMn} measured at 300 K are displayed in Fig. 5(a). The Co/Fe/Cu film alone shows only in-plane magnetic anisotropy. However, PMA was observed in Fe₅₀Mn₅₀/Co/Fe/Cu when t_{FeMn} is greater than 8 ML. To comprehend the relationship between the induced PMA in Fe₅₀Mn₅₀/Co/Fe/Cu and the antiferromagnetism of the Fe₅₀Mn₅₀ films, it was of utmost importance to identify the initiation of long-range AFM ordering within the Fe₅₀Mn₅₀ films. Previous studies [45–48] utilized x-ray magnetic linear dichroism (XMLD) as a direct method for examining the long-range AFM order in AFM films. However, obtaining distinguishable XMLD spectra for the current AFM films was challenging due to the fixed orientation between the x-ray and sample holder and the full magnetic shielding in the sample holder of the PEEM [42]. Therefore, in this work, we characterized the onset of long-range AFM ordering in the Fe₅₀Mn₅₀ or Mn films by observing the fingerprintlike phenomenon of increased H_c in the coupled AFM/FM systems due to AFM-induced exchange coupling. This approach has been justified in numerous previous AFM/FM thin film studies [3,8,43,44]. As displayed in Figs. 5(c) and 5(d), the strong enhancement of H_c was observed when $t_{\text{FeMn}} > 8$ ML. This behavior suggests that long-range AFM ordering of Fe₅₀Mn₅₀ films is established when $t_{\text{FeMn}} > 8$ ML. Thus, the PMA induction induced

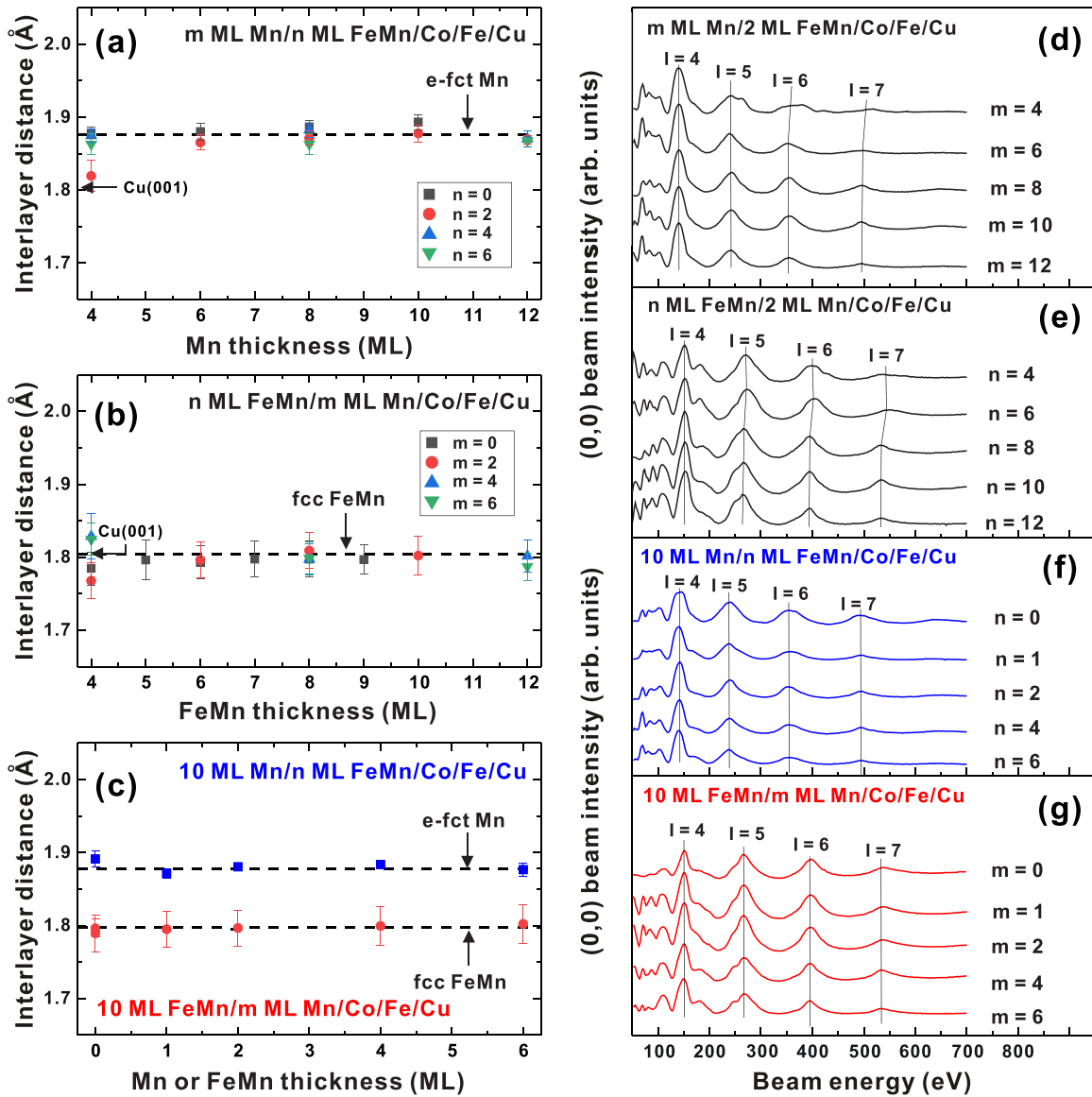


FIG. 4. The average interlayer distance d_{\perp} of (a) various Mn films grown on 0–6-ML $\text{Fe}_{50}\text{Mn}_{50}/\text{Co}/\text{Fe}/\text{Cu}$ and (b) various $\text{Fe}_{50}\text{Mn}_{50}$ films grown on 0–6-ML Mn/Co/Fe/Cu, as calculated according to the energy peaks (I) of the corresponding LEED specular spot I/V curves in (d) and (e), respectively, measured at 300 K. (c) d_{\perp} of 10-ML Mn grown on 0–6-ML $\text{Fe}_{50}\text{Mn}_{50}/\text{Co}/\text{Fe}/\text{Cu}$ and 10-ML $\text{Fe}_{50}\text{Mn}_{50}$ grown on 0–6-ML Mn/Co/Fe/Cu calculated according to LEED I/V curves in (f) and (g), respectively, measured at 300 K.

when $t_{\text{FeMn}} > 8$ ML could be attributable to the AFM-induced exchange coupling from the AFM $\text{Fe}_{50}\text{Mn}_{50}$ layer, probably caused by the presence of out-of-plane uncompensated spin components at the AFM-FM interface [Fig. 1(a)] [30].

As another structurally compatible AFM-FM exchange-coupled system, the magnetic hysteresis loops of the 0–10-ML Mn/Co/Fe/Cu measured at 300 K are also displayed in Fig. 5(b). However, as the in-plane magnetization of Mn/Co/Fe/Cu decreases significantly when t_{Mn} is greater than 4 ML, only very small perpendicular magnetization is seen in the out-of-plane hysteresis loops [Fig. 5(e)]. Moreover, the small perpendicular magnetization is further reduced when t_{Mn} is greater than 8 ML. Note that an enhancement of the H_c value was observed in Mn/Co/Fe/Cu when t_{Mn} was greater than 4 ML [Fig. 5(e)]. This finding suggests the establishment of long-range AFM ordering of Mn films

when $t_{\text{Mn}} > 4$ ML, similar to the observation in a previous report [49]. Such a small perpendicular magnetization observed at $t_{\text{Mn}} = 6, 8$ ML but then reduced at $t_{\text{Mn}} = 10$ ML in Mn/Co/Fe/Cu could be attributed to the competition between the established perpendicular interface crystalline anisotropy of the interfacial Mn/Co moments [15,17] and the in-plane exchange coupling from the in-plane-oriented spin moments of the Mn film [Fig. 1(b)] [36,37], as explained in detail in a previous report [30].

C. PMA induction in Mn/ $\text{Fe}_{50}\text{Mn}_{50}/\text{Co}/\text{Fe}/\text{Cu}$

To explore the effects of applying AFM composite films on PMA induction of adjacent FM films, the stacking structure of Mn/ $\text{Fe}_{50}\text{Mn}_{50}/\text{Co}/\text{Fe}/\text{Cu}$, where the $\text{Fe}_{50}\text{Mn}_{50}$ film is in contact with Co/Fe/Cu, is further investigated.

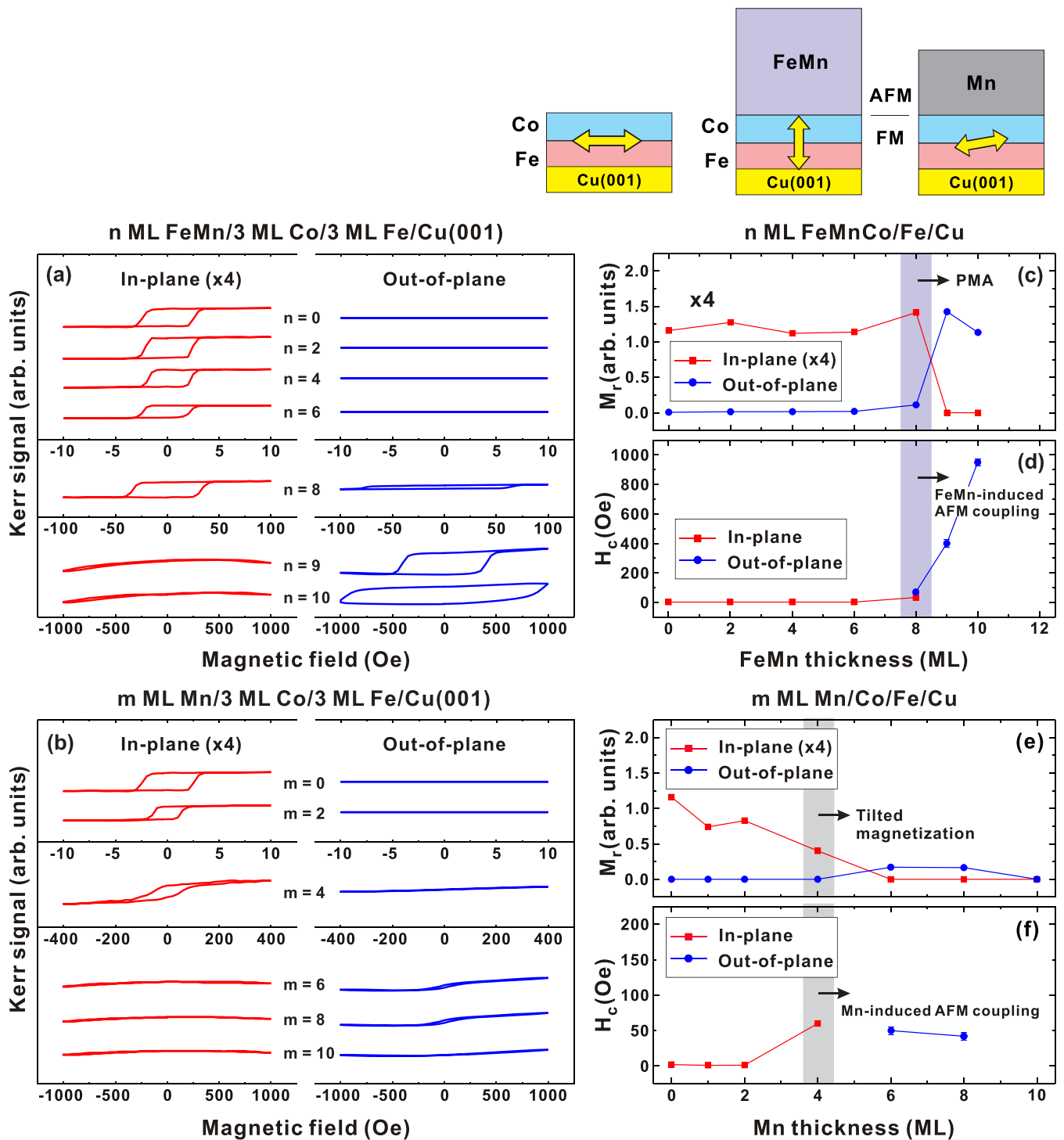


FIG. 5. Magnetic hysteresis loops of (a) 0–10-ML $\text{Fe}_{50}\text{Mn}_{50}/\text{Co}/\text{Fe}/\text{Cu}$ and (b) 0–10-ML $\text{Mn}/\text{Co}/\text{Fe}/\text{Cu}$ measured using longitudinal and polar MOKE at 300 K. (c)–(f) The summarized values of M_r and H_c obtained from the magnetic hysteresis loops in (a) and (b). In (c) and (d), the blue shaded regions represent a similar threshold thickness of t_{FeMn} (≈ 8 ML) that marks the onset of induced PMA and the establishment of FeMn-induced AFM-FM exchange coupling in $\text{Fe}_{50}\text{Mn}_{50}/\text{Co}/\text{Fe}/\text{Cu}$. In (e) and (f), the gray shaded regions indicate a similar threshold thickness of t_{Mn} (≈ 4 ML) that indicates the onset of induced tilted magnetization and Mn-induced AFM-FM exchange coupling in $\text{Mn}/\text{Co}/\text{Fe}/\text{Cu}$.

Figure 6(a) displays the magnetic hysteresis loops of 0–12-ML $\text{Mn}/\text{Fe}_{50}\text{Mn}_{50}/\text{Co}/\text{Fe}/\text{Cu}$ with t_{FeMn} fixed at 2 ML. The 2-ML $\text{Fe}_{50}\text{Mn}_{50}/\text{Co}/\text{Fe}/\text{Cu}$ exhibits in-plane magnetic anisotropy. When the Mn film with $t_{\text{Mn}} > 4$ ML is added on top of 2-ML $\text{Fe}_{50}\text{Mn}_{50}/\text{Co}/\text{Fe}/\text{Cu}$, PMA with enhanced

perpendicular H_c is observed [Figs. 6(c) and 6(d)]. In Mn/2-ML $\text{Fe}_{50}\text{Mn}_{50}/\text{Co}/\text{Fe}/\text{Cu}$, the threshold value of t_{Mn} for the PMA induction and enhanced H_c is close to the onset of AFM ordering of the Mn film in $\text{Mn}/\text{Co}/\text{Fe}/\text{Cu}$ [$t_{\text{Mn}} \approx 4$ ML; Fig. 5(f)]. This finding provides evidence that the PMA in

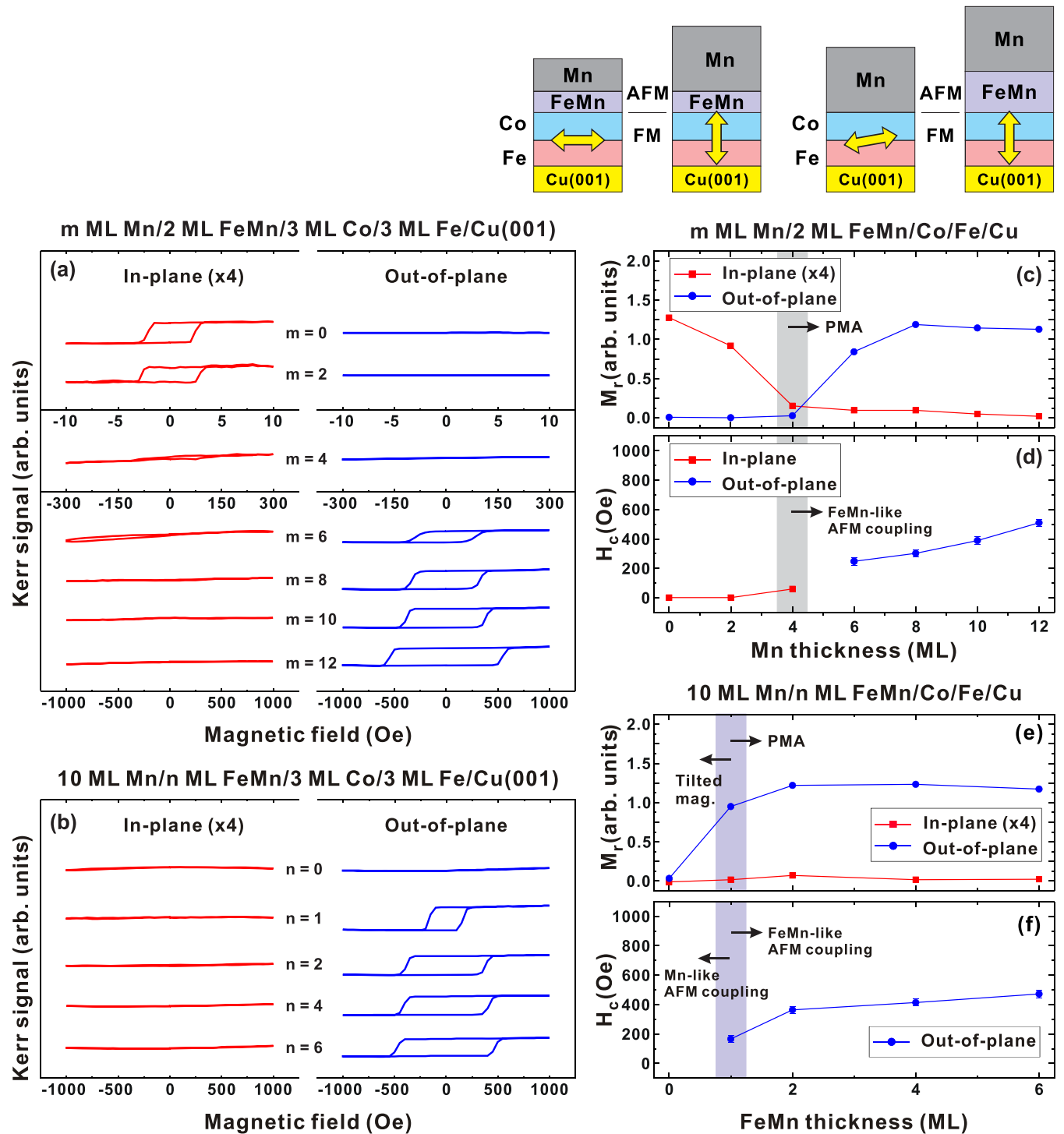


FIG. 6. Magnetic hysteresis loops of (a) 0–12-ML Mn/2-ML $\text{Fe}_{50}\text{Mn}_{50}$ /Co/Fe/Cu and (b) 10-ML Mn/0–6-ML $\text{Fe}_{50}\text{Mn}_{50}$ /Co/Fe/Cu films measured using longitudinal and polar MOKE at 300 K. (c)–(f) The summarized values of M_r and H_c obtained from the magnetic hysteresis loops in (a) and (b). In (c) and (d), the gray shaded regions indicate a similar threshold thickness (≈ 4 ML) that signifies the onset of induced PMA and FeMn-like AFM-FM exchange coupling in Mn/2-ML $\text{Fe}_{50}\text{Mn}_{50}$ /Co/Fe/Cu. In (e) and (f), the blue shaded regions represent the estimated threshold thicknesses of t_{FeMn} (≈ 1 ML) that mark the onset of induced PMA and the transition from Mn-like to FeMn-like AFM-FM exchange coupling.

Mn/2-ML $\text{Fe}_{50}\text{Mn}_{50}$ /Co/Fe/Cu could be assisted by the top Mn films with established long-range AFM ordering through the AFM exchange coupling at the Mn- $\text{Fe}_{50}\text{Mn}_{50}$ interface.

To better understand the impact of the thickness of the $\text{Fe}_{50}\text{Mn}_{50}$ spacer layer on PMA induction in the

Mn/ $\text{Fe}_{50}\text{Mn}_{50}$ /Co/Fe/Cu system, we varied t_{FeMn} of the $\text{Fe}_{50}\text{Mn}_{50}$ spacer layer while keeping the thickness of the top-most Mn layer at 10 ML to maintain its AFM state. As shown in Figs. 6(b), 6(e), and 6(f), the magnetization of 10-ML Mn/ $\text{Fe}_{50}\text{Mn}_{50}$ /Co/Fe/Cu changed from an unsaturated to

a fully saturated perpendicular magnetic state when $t_{\text{FeMn}} \geq 1$ ML. Interestingly, the values of perpendicular H_c induced in 10-ML Mn/2–6-ML Fe₅₀Mn₅₀/Co/Fe/Cu [Fig. 6(f)] and 9-ML Fe₅₀Mn₅₀/Co/Fe/Cu [Fig. 5(d)] are on a similar level ($H_c \approx 400$ –500 Oe). This finding suggests that the composite 10-ML Mn/2–6-ML Fe₅₀Mn₅₀ films could create an FeMn-like interfacial coupling on adjacent Co/Fe/Cu, even though thin Fe₅₀Mn₅₀ spacer layers ($t_{\text{FeMn}} = 2$ –6 ML) at the AFM-FM interface are applied. However, according to Figs. 5(a) and 5(c), a single Fe₅₀Mn₅₀ film reaches the AFM state when t_{FeMn} is greater than 8 ML. Thus, the presence of FeMn-like AFM-FM exchange coupling in 10-ML Mn/1–6-ML Fe₅₀Mn₅₀/Co/Fe/Cu suggests that the topmost 10-ML Mn film could promote the long-range AFM ordering of the thin Fe₅₀Mn₅₀ spacer layer through Mn-Fe₅₀Mn₅₀ exchange coupling; this demonstrates one example in which the AFM proximity effect within the composite Mn/Fe₅₀Mn₅₀ system could help to trigger PMA in the adjacent Co/Fe/Cu layer.

D. PMA induction in Fe₅₀Mn₅₀/Mn/Co/Fe/Cu

To explore other possibilities of proximity effects within AFM composite films that are helpful for the PMA induction in adjacent FM films, we further study Fe₅₀Mn₅₀/Mn/Co/Fe/Cu, where the Mn layer is in contact with Co/Fe/Cu. Figure 7(a) displays the 0–10-ML Fe₅₀Mn₅₀/Mn/Co/Fe/Cu with a fixed 2-ML Mn layer at the AFM-FM interface; 2-ML Mn/Co/Fe/Cu alone reveals only in-plane magnetic anisotropy. Note that the in-plane (out-of-plane) magnetization of Fe₅₀Mn₅₀/2-ML Mn/Co/Fe/Cu decreases (weakly increases) when t_{FeMn} reaches 4–6 ML. This result is similar to the magnetic behavior observed in Mn/Co/Fe/Cu when t_{Mn} reaches 4–6 ML [Fig. 5(b)] and thus suggests the presence of Mn-like exchange coupling at the AFM-FM interface of 4–6-ML Fe₅₀Mn₅₀/2-ML Mn/Co/Fe/Cu. Moreover, this finding also indicates that the top 4–6-ML Fe₅₀Mn₅₀ could aid the long-range AFM ordering of the 2-ML Mn spacer layer through a mutual exchange interaction, even if the thickness of either the Fe₅₀Mn₅₀ or Mn film is lower than its threshold for the establishment of long-range AFM ordering (≈ 8 ML for Fe₅₀Mn₅₀ [Fig. 5(d)] and ≈ 4 ML for Mn [Fig. 5(f)]). However, when t_{FeMn} in Fe₅₀Mn₅₀/2-ML Mn/Co/Fe/Cu is higher than 8 ML, where the Fe₅₀Mn₅₀ film is in a robust AFM state, stable PMA can further be induced [Fig. 7(a)]. This behavior is similar to the PMA induction in Fe₅₀Mn₅₀/Co/Fe/Cu [Fig. 5(a)] and thus also suggests the presence of FeMn-like AFM coupling at the AFM-FM interface of 8–10-ML Fe₅₀Mn₅₀/2-ML Mn/Co/Fe/Cu, even though the spacer layer is a Mn film.

To better understand the impact of Mn spacer layer thickness on PMA induction in the Fe₅₀Mn₅₀/Mn/Co/Fe/Cu system, we systematically changed t_{Mn} of the Mn spacer layer while keeping t_{FeMn} at 10 ML to maintain a robust AFM state of the topmost Fe₅₀Mn₅₀ film. As shown in Figs. 7(b) and 7(f), PMA with sizable H_c is observed in the 10-ML Fe₅₀Mn₅₀/Mn/Co/Fe/Cu when t_{Mn} is less than 4 ML, again revealing an FeMn-like AFM-FM exchange coupling at the AFM-FM interface. However, when t_{Mn} in the 10-ML Fe₅₀Mn₅₀/Mn/Co/Fe/Cu is larger than 4 ML, the induced PMA in 10-ML Fe₅₀Mn₅₀/Mn/Co/Fe/Cu is significantly

reduced, restoring the behavior of Mn-like AFM-FM exchange coupling to that observed in Mn/Co/Fe/Cu [Fig. 5(b)]; this behavior could be attributed to the establishment of robust long-range AFM ordering of the Mn spacer layer ($t_{\text{Mn}} \approx 4$ ML).

E. AFM-FM interface coupling triggered by AFM composite films

To understand the underlying cause of the induced PMA in Mn/Fe₅₀Mn₅₀/Co/Fe/Cu and Fe₅₀Mn₅₀/Mn/Co/Fe/Cu films, the interface coupling is further investigated through Co, Fe, and Mn $L_{3,2}$ XAS and XMCD measurements. In this study, XMCD signals were measured using fixed x-ray circular polarization while flipping the magnetic moments with out-of-plane magnetic fields. Consequently, the XMCD signal from the Mn element is expected to primarily originate from Mn moments near the AFM-FM interface. These Mn moments are coupled to the FM moments and exhibit flipping behavior in response to the applied magnetic field.

Figures 8(a)–8(c) show the $L_{3,2}$ XAS and XMCD curves for the Co, Fe, and Mn elements in the 10-ML Fe₅₀Mn₅₀/Co/Fe/Cu film. This film serves as a standard sample, demonstrating PMA and FeMn-like exchange coupling at the AFM-FM interface [see Fig. 5(a)]. The Co, Fe, and Mn elements display XMCD asymmetries with the same sign, indicating collinear- and parallel-like coupling between the FM moments and the uncompensated Mn moments in the out-of-plane direction of the AFM-FM interface. This coupling can be attributed to the 3Q spin structure of the Fe₅₀Mn₅₀ films [Fig. 1(a)] [16,30], which could be the origin of the induced PMA in the 10-ML Fe₅₀Mn₅₀/Co/Fe/Cu film.

In prior research on the Fe₅₀Mn₅₀/Co/Cu(001) system, Offi *et al.* [50] discovered that a net magnetic moment in both Fe and Mn can be induced by an adjacent FM layer, irrespective of the paramagnetic (PM) or AFM state of the Fe₅₀Mn₅₀ thin films. However, their findings also indicated that the magnetic moment configuration induced in AFM Fe₅₀Mn₅₀ remains closely associated with its 3Q AFM spin structure. In the present Fe₅₀Mn₅₀/Co/Fe/Cu system, we speculate that when Fe₅₀Mn₅₀ transitions from a PM to an AFM state, the perpendicular magnetization induced at this juncture might also polarize the out-of-plane-oriented uncompensated moment of AFM Fe₅₀Mn₅₀ through the proximity effect. Consequently, this process further enhances the collinearlike coupling at the FeMn-FM interface and reinforces the established perpendicular magnetization. By contrast, for Mn/Co/Fe/Cu or Mn/Co/Ni/Cu systems that generate perpendicular magnetization via noncollinear AFM-FM coupling, the induced magnetic moment in the AFM layer is notably weaker, as demonstrated in previous reports [17,30].

Regarding Figs. 8(d)–8(f), it is noteworthy that the Mn elements in both the PMA-established 4-ML Mn/4-ML Fe₅₀Mn₅₀/Co/Fe/Cu and 10-ML Fe₅₀Mn₅₀/2-ML Mn/Co/Fe/Cu systems exhibit also the same sign and XMCD asymmetry similar to the 10-ML Fe₅₀Mn₅₀/Co/Fe/Cu system. This finding provides confirmation that the FeMn-like AFM coupling at the AFM-FM interfaces is responsible for

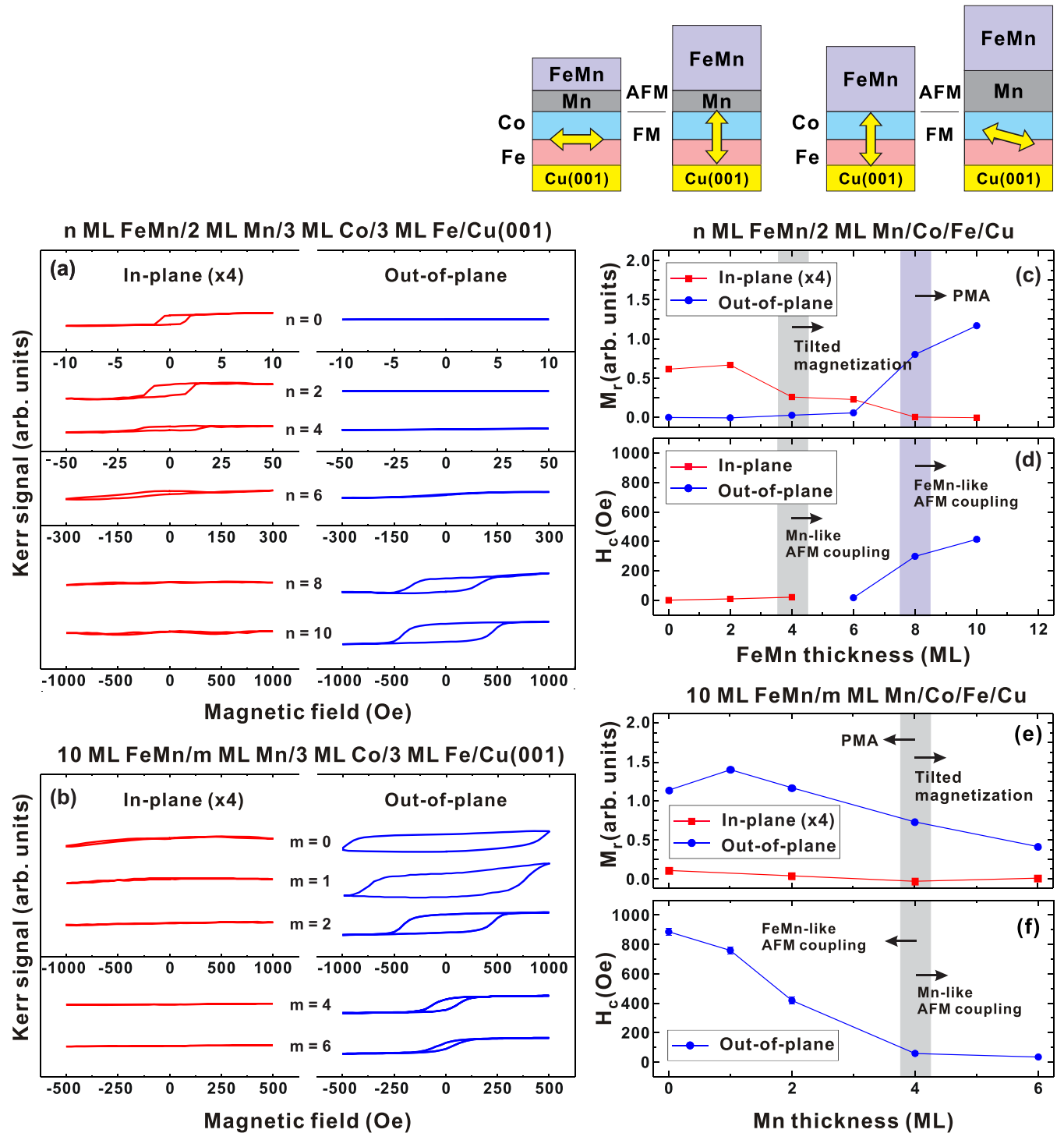


FIG. 7. Magnetic hysteresis loops of (a) 0–10-ML $\text{Fe}_{50}\text{Mn}_{50}$ /2-ML Mn/Co/Cu and (b) 10-ML $\text{Fe}_{50}\text{Mn}_{50}$ /0–6 ML Mn/Co/Fe/Cu films measured at 300 K using longitudinal and polar MOKE. (c)–(f) The summarized values of M_r and H_c obtained from the magnetic hysteresis loops in (a) and (b). In (c), the gray and blue shaded regions represent the threshold thicknesses for the onset of induced tilted magnetization ($t_{\text{FeMn}} \approx 4$ ML) and PMA ($t_{\text{FeMn}} \approx 8$ ML), respectively. These values are similar to the critical thicknesses for the established Mn- and FeMn-like AFM-FM coupling in $\text{Fe}_{50}\text{Mn}_{50}$ /2-ML Mn/Co/Fe/Cu as shown in (d). In (e) and (f), the gray shaded regions indicate a similar threshold thickness of $t_{\text{Mn}} (\approx 4$ ML) that corresponds to the onset of induced tilted magnetization and a transition from FeMn- to Mn-like AFM-FM exchange coupling in 10-ML $\text{Fe}_{50}\text{Mn}_{50}$ /Mn/Co/Fe/Cu.

the induced PMA in both systems. Based on the aforementioned results, we have obtained a much clearer understanding that in the Mn/ $\text{Fe}_{50}\text{Mn}_{50}$ /Co/Fe/Cu structure, the topmost AFM Mn films can stabilize the long-range AFM ordering

of the thin $\text{Fe}_{50}\text{Mn}_{50}$ spacer layer [Fig. 8(g)]. This stabilization leads to the generation of FeMn-like AFM-FM coupling and induces PMA in the Co/Fe/Cu layers. Furthermore, in the $\text{Fe}_{50}\text{Mn}_{50}$ /Mn/Co/Fe/Cu structure, the topmost AFM

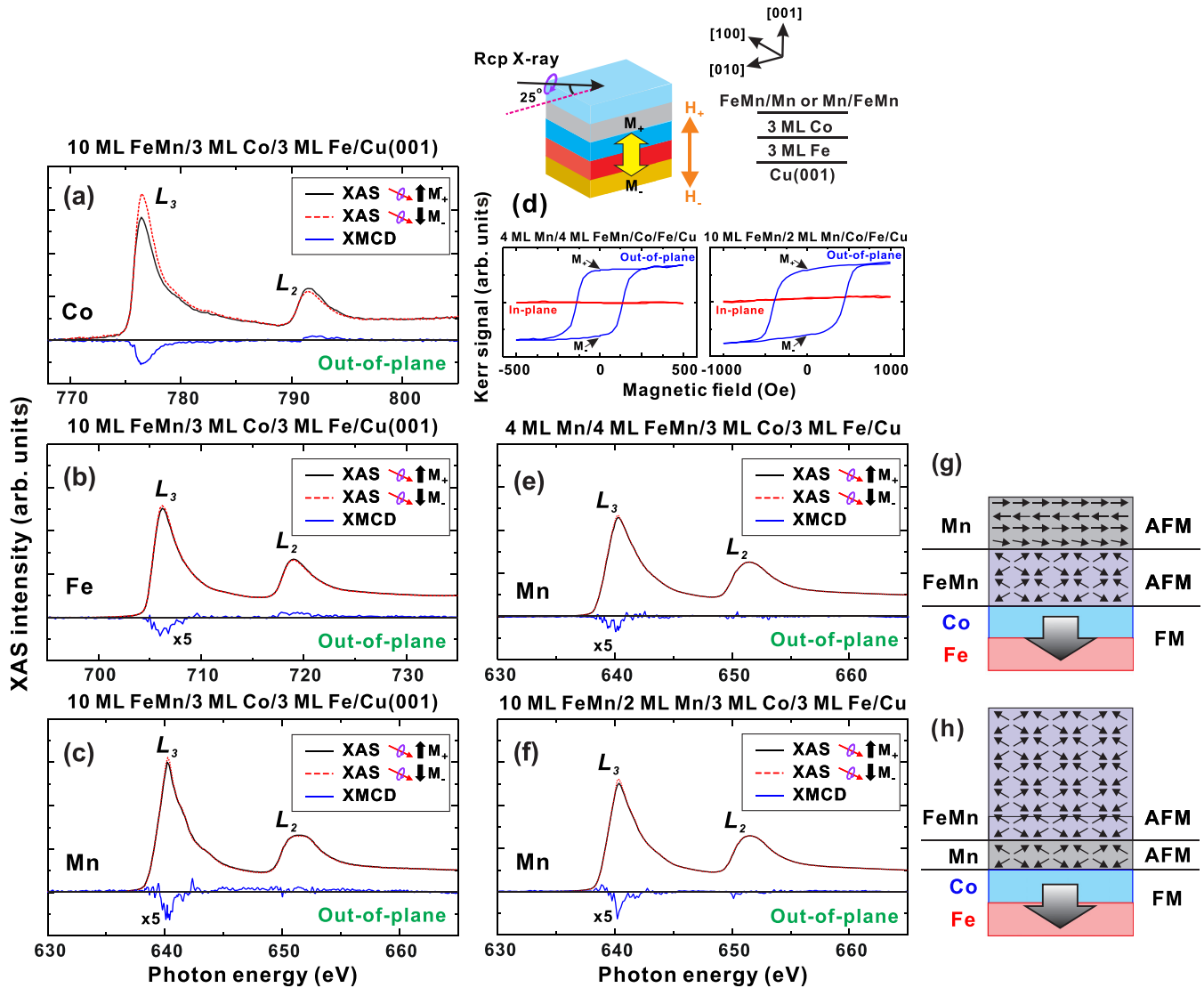


FIG. 8. (a)–(c) XAS and XMCD curves of 10-ML $\text{Fe}_{50}\text{Mn}_{50}/\text{Co}/\text{Fe}/\text{Cu}$ measured at the (a) Co, (b) Fe, and (c) Mn $L_{3,2}$ edges at 300 K in remanent states. (d) In-plane and out-of-plane magnetic hysteresis loops of 4-ML Mn/4-ML $\text{Fe}_{50}\text{Mn}_{50}/\text{Co}/\text{Fe}/\text{Cu}$ and 10-ML $\text{Fe}_{50}\text{Mn}_{50}/2\text{-ML Mn}/\text{Co}/\text{Cu}$ measured at 300 K. The black arrows (M_+ or M_-) indicate the remanent states of the films under positive (H_+) or negative (H_-) magnetic field. XAS and XMCD curves of (e) 4-ML Mn/4-ML $\text{Fe}_{50}\text{Mn}_{50}/\text{Co}/\text{Fe}/\text{Cu}$ and (f) 10-ML $\text{Fe}_{50}\text{Mn}_{50}/2\text{-ML Mn}/\text{Co}/\text{Cu}$ measured at the Mn $L_{3,2}$ edge at 300 K in remanent states. Schematic illustrations of the possible AFM spin configurations in the films of (g) PMA-established 4-ML Mn/4-ML $\text{Fe}_{50}\text{Mn}_{50}/\text{Co}/\text{Fe}/\text{Cu}$ and (h) 10-ML $\text{Fe}_{50}\text{Mn}_{50}/2\text{-ML Mn}/\text{Co}/\text{Cu}$.

$\text{Fe}_{50}\text{Mn}_{50}$ film can even polarize the AFM spin structure of the thin Mn spacer layer [Fig. 8(h)]. This polarization effect subsequently triggers PMA in the Co/Fe/Cu layers through FeMn-like AFM coupling at the AFM-FM interface.

IV. DISCUSSION

A. PMA induction by AFM composite films and the roles of AFM proximity effects

The results above have provided evidence that the AFM-FM coupling behaviors induced by composite AFM films are highly sensitive to the thickness as well as the strength of AFM ordering of the individual AFM layer. To trace the AFM-FM coupling and PMA generated by these composite AFM films, we conducted systematic measurements of the

magnetic hysteresis loops for Mn/ $\text{Fe}_{50}\text{Mn}_{50}/\text{Co}/\text{Fe}/\text{Cu}$ and $\text{Fe}_{50}\text{Mn}_{50}/\text{Mn}/\text{Co}/\text{Fe}/\text{Cu}$ while varying t_{Mn} and t_{FeMn} . The results are summarized in the magnetic easy axis phase diagrams depicted in Fig. 9.

Figure 9(a) displays the magnetic easy axis phase diagrams of Mn/ $\text{Fe}_{50}\text{Mn}_{50}/\text{Co}/\text{Fe}/\text{Cu}$. AFM Mn/Co/Fe/Cu ($t_{\text{Mn}} > 4$ ML) does not induce stable PMA, in which the coupling at the AFM-FM interface can be classified as the Mn-like AFM coupling. When an $\text{Fe}_{50}\text{Mn}_{50}$ spacer layer is included between Mn and Co/Fe/Cu, both PMA and FeMn-like AFM coupling can be triggered, as seen in the blue shaded area in Fig. 9(a). Note that in Mn/ $\text{Fe}_{50}\text{Mn}_{50}/\text{Co}/\text{Fe}/\text{Cu}$, the threshold of t_{Mn} for triggering PMA is reduced when t_{FeMn} of the $\text{Fe}_{50}\text{Mn}_{50}$ spacer layer is increased, indicating that a thicker (thinner) $\text{Fe}_{50}\text{Mn}_{50}$ spacer layer requires a thinner (thicker) Mn capping

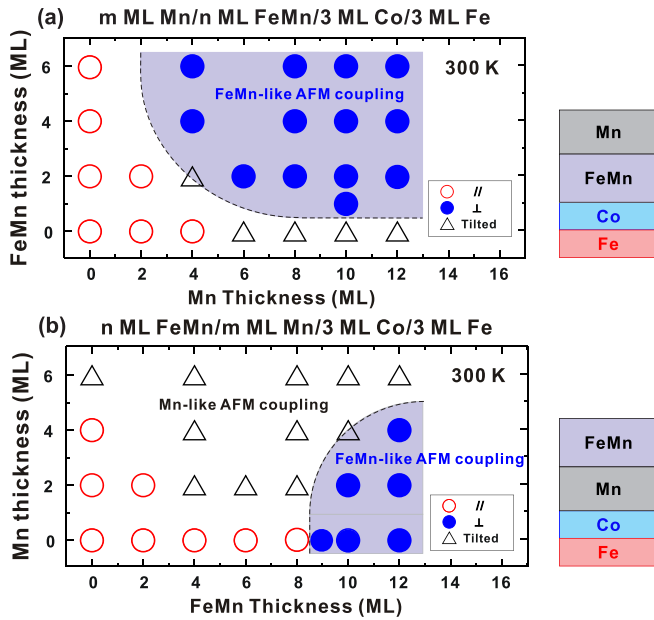


FIG. 9. Magnetic easy axis phase diagrams of the (a) Mn/Fe₅₀Mn₅₀/Co/Fe/Cu and (b) Fe₅₀Mn₅₀/Mn/Co/Fe/Cu systems plotted as a function of t_{Mn} and t_{FeMn} at 300 K based on longitudinal and polar MOKE measurements. The // (\perp) symbol indicates the in-plane (perpendicular) magnetic easy axis of the films, while the triangle represents tilted or canted magnetization. The dashed lines represent the boundary between the perpendicular and in-plane (or tilted) magnetizations of the films. In (a) and (b), the blue shaded regions indicate the thickness range where FeMn-like AFM couplings are observed in Mn/Fe₅₀Mn₅₀/Co/Fe/Cu and Fe₅₀Mn₅₀/Mn/Co/Fe/Cu, respectively. The triangles signify the presence of a tilted magnetic state and Mn-like AFM coupling.

film to achieve the AFM state of Fe₅₀Mn₅₀. This behavior demonstrates the presence of finite-size-like effects [20] in the AFM composite Mn/Fe₅₀Mn₅₀ films when the thickness of the individual AFM layer is varied, similar to what is commonly observed in a single AFM film when the film thickness is altered [20]. Thus, in Mn/Fe₅₀Mn₅₀/Co/Fe/Cu, we can confirm that the topmost Mn film could promote the long-range AFM ordering of the Fe₅₀Mn₅₀ spacer layer through such an AFM proximity effect; this effect therefore triggers PMA in adjacent Co/Fe/Cu through the formation of FeMn-like exchange coupling at the AFM-FM interface, like what we observed in the XMCD data [Figs. 8(c) and 8(e)].

On the other hand, Fig. 9(b) displays the magnetic easy axis phase diagram of Fe₅₀Mn₅₀/Mn/Co/Fe/Cu at room temperature for different t_{FeMn} and t_{Mn} . AFM Fe₅₀Mn₅₀/Co/Fe/Cu with $t_{\text{FeMn}} > 8$ ML can induce strong PMA as well as FeMn-like AFM coupling on the adjacent Co/Fe/Cu film at room temperature. However, incorporating an Mn spacer layer between Fe₅₀Mn₅₀ and Co/Fe/Cu reduces PMA and revives Mn-like AFM coupling. In Fe₅₀Mn₅₀/Mn/Co/Fe/Cu, applying a thicker Mn spacer layer requires a higher t_{FeMn} value to trigger stable PMA, indicating a competitive relationship between the FeMn- and Mn-like AFM couplings at the AFM-FM interface of Fe₅₀Mn₅₀/Mn/Co/Fe/Cu. Moreover, since the Mn layer is located at the AFM-FM interface of Fe₅₀Mn₅₀/Mn/Co/Fe/Cu, it is unlikely that PMA can

be triggered solely by enhancing the AFM ordering temperature of the Mn spacer layer; this effect is expected to generate Mn-like exchange coupling at the AFM-FM interface [Fig. 5(b)]. Therefore, there must be another type of AFM proximity effect present in Fe₅₀Mn₅₀/Mn/Co/Fe/Cu to account for the presence of PMA, as well as FeMn-like AFM coupling at the AFM-FM interface. Indeed, based on XMCD experiments, we observe an uncompensated Mn magnetic moment signal in a 10-ML Fe₅₀Mn₅₀/2-ML Mn/Co/Fe/Cu structure with PMA [Fig. 8(f)]. This property closely resembles the behavior of the 10-ML Fe₅₀Mn₅₀/Co/Fe/Cu and 4-ML Mn/4-ML Fe₅₀Mn₅₀/Co/Fe/Cu structures, which exhibit FeMn-like coupling and PMA induction. Therefore, in the PMA-established Fe₅₀Mn₅₀/Mn/Co/Fe/Cu structure, we postulate that the topmost AFM Fe₅₀Mn₅₀ film can polarize the AFM spin structure of the thin Mn spacer layer [Fig. 8(h)], leading to the generation of FeMn-like coupling and PMA in the adjacent Co/Fe/Cu film. This discovery unveils another example of the AFM proximity effect between AFM layers.

B. Absence of Mn-like AFM coupling in AFM Mn/Fe₅₀Mn₅₀/Co/Fe/Cu

Based on the earlier XMCD results [Fig. 8(f)], it is evident that the AFM Fe₅₀Mn₅₀ film has the ability to polarize a thin Mn spacer layer, resulting in FeMn-like AFM coupling and PMA in the Co/Fe/Cu film. However, in the case of AFM Mn/Fe₅₀Mn₅₀/Co/Fe/Cu, only PMA or FeMn-like AFM coupling was observed, despite the Fe₅₀Mn₅₀ spacer layer being very thin [$t_{\text{FeMn}} = 1$ ML; Figs. 6(b) and 9(a)]. Consequently, it appears that Mn-like AFM coupling is absent in Mn/Fe₅₀Mn₅₀/Co/Fe/Cu. In fact, although the AFM Mn film alone can induce only tilted magnetization in Co/Fe/Cu in the present work [Fig. 5(b)], it can induce robust PMA in the adjacent FM film under certain conditions, such as a lower in-plane anisotropy of the FM film [15] or enhanced perpendicular interface anisotropy at low temperatures [30]. Thus, in the case of AFM Mn/Fe₅₀Mn₅₀/Co/Fe/Cu, we infer that the thin Fe₅₀Mn₅₀ spacer layer may still possess some out-of-plane spin components when coupled with the in-plane-oriented Mn moments within the Mn film volume [36,37]. These out-of-plane spin components of Fe₅₀Mn₅₀ moments can contribute to the FeMn-like AFM coupling and therefore aid in stabilizing the PMA of the underlying Co/Fe/Cu film. Therefore, even with a thin Fe₅₀Mn₅₀ spacer layer, both stable PMA and FeMn-like AFM coupling are present in Mn/Fe₅₀Mn₅₀/Co/Fe/Cu system.

C. Triggering PMA in Fe₅₀Mn₅₀/Mn/Co/Fe/Cu via a long-range FeMn exchange coupling through the Mn spacer layer?

Based on the results above (Fig. 7), it was observed that both PMA and FeMn-like AFM coupling can be induced in Fe₅₀Mn₅₀/Mn/Co/Fe/Cu when t_{Mn} of the Mn spacer layer is below 4 ML, which is considered the threshold value for establishing long-range AFM ordering of Mn in Mn/Co/Fe/Cu. This finding raises the question of whether the Mn spacer layer in Fe₅₀Mn₅₀/Mn/Co/Fe/Cu remains in a paramagnetic state. If so, does the topmost layer of Fe₅₀Mn₅₀ films induce

PMA and FeMn-like AFM coupling in the FM film through the Mn spacer layer via a Ruderman-Kittel-Kasuya-Yosida-like long-range coupling [51–55]? In fact, as demonstrated for Fe₅₀Mn₅₀/2-ML Mn/Co/Fe/Cu [Figs. 7(c) and 7(d)], the coupling effects on the FM film exhibit variations from Mn-like to FeMn-like AFM coupling when t_{FeMn} of the Fe₅₀Mn₅₀ spacer layer is increased from 4–6 ML to 8 ML. This indicates that the 2-ML Mn spacer layer in the PMA-established Fe₅₀Mn₅₀/Mn/Co/Fe/Cu system should not be considered paramagnetic. Therefore, the possibility of triggering PMA in Fe₅₀Mn₅₀/Mn/Co/Fe/Cu through long-range exchange coupling between Fe₅₀Mn₅₀ and Co/Fe/Cu should be excluded.

V. CONCLUSION

We have conducted a comprehensive investigation into the effects of inducing PMA in FM Co/Fe/Cu films by utilizing AFM composite layers of Mn/Fe₅₀Mn₅₀ or Fe₅₀Mn₅₀/Mn. Our results demonstrate that in the Mn/Fe₅₀Mn₅₀/Co/Fe/Cu structure, the top AFM Mn film enhances the long-range AFM ordering of the thin Fe₅₀Mn₅₀ spacer layer, resulting in

the induction of FeMn-like AFM coupling and PMA in the Co/Fe/Cu film. In addition, in the Fe₅₀Mn₅₀/Mn/Co/Fe/Cu structure, our findings indicate that the AFM Fe₅₀Mn₅₀ film not only enhances the long-range AFM ordering but also modulates the AFM spin structure of the adjacent Mn spacer layer. This modulation triggers FeMn-like AFM coupling and PMA in the adjacent Co/Fe/Cu films. Our research has unveiled the capabilities of AFM proximity effects, enhancing our understanding of AFM state control. These proposed mechanisms can be extrapolated to other AFM composite layers that involve AFM films with different AFM ordering temperatures or spin structures, offering flexible control over antiferromagnet-induced PMA. Moreover, these research results have the potential to inspire the application of PMA in next-generation perpendicular spintronic devices that utilize AFM composite films with diverse AFM spin structures.

ACKNOWLEDGMENT

This work was partly supported by the National Science and Technology Council, Taiwan (Grant No. NSTC 112-2112-M-018-006).

- [1] W. H. Meiklejohn and C. P. Bean, *Phys. Rev.* **102**, 1413 (1956).
- [2] W. H. Meiklejohn and C. P. Bean, *Phys. Rev.* **105**, 904 (1957).
- [3] J. Nogués and I. K. Schuller, *J. Magn. Magn. Mater.* **192**, 203 (1999).
- [4] S. D. Bader, *Rev. Mod. Phys.* **78**, 1 (2006).
- [5] P. S. Mao, Z. Gao, H. Xi, P. Kolbo, M. Plumer, L. Wang, A. Goyal, I. Jin, J. Chen, C. Hou, R. M. White, and E. Murdock, *IEEE Trans. Magn.* **38**, 26 (2002).
- [6] H. Ohldag, A. Scholl, F. Nolting, S. Anders, F. U. Hillebrecht, and J. Stöhr, *Phys. Rev. Lett.* **86**, 2878 (2001).
- [7] W. Kuch, F. Offi, L. I. Chelaru, M. Kotsugi, K. Fukumoto, and J. Kirschner, *Phys. Rev. B* **65**, 140408(R) (2002).
- [8] C. Won, Y. Z. Wu, H. W. Zhao, A. Scholl, A. Doran, W. Kim, T. L. Owens, X. F. Jin, and Z. Q. Qiu, *Phys. Rev. B* **71**, 024406 (2005).
- [9] Q. F. Zhan and K. M. Krishnan, *Appl. Phys. Lett.* **96**, 112506 (2010).
- [10] B. Y. Wang, C. H. Chuang, S. S. Wong, J. J. Chiou, W. C. Lin, Y. L. Chan, D. H. Wei, and M. T. Lin, *Phys. Rev. B* **85**, 094412 (2012).
- [11] B. Y. Wang, N. Y. Jih, W. C. Lin, C. H. Chuang, P. J. Hsu, C. W. Peng, Y. C. Yeh, Y. L. Chan, D. H. Wei, W. C. Chiang, and M. T. Lin, *Phys. Rev. B* **83**, 104417 (2011).
- [12] B. Y. Wang, J. Y. Hong, K. H. O. Yang, Y. L. Chan, D. H. Wei, H. J. Lin, and M. T. Lin, *Phys. Rev. Lett.* **110**, 117203 (2013).
- [13] P. Kuświk, P. L. Gastelois, M. M. Soares, H. C. N. Tolentino, M. De Santis, A. Y. Ramos, A. D. Lamirand, M. Przybylski, and J. Kirschner, *Phys. Rev. B* **91**, 134413 (2015).
- [14] P. Kuświk, B. Szymański, B. Anastaziak, M. Matczak, M. Urbaniak, A. Ehresmann, and F. Stobiecki, *J. Appl. Phys.* **119**, 215307 (2016).
- [15] B.-Y. Wang, P.-H. Lin, M.-S. Tsai, C.-W. Shih, M.-J. Lee, C.-W. Huang, N.-Y. Jih, P.-Y. Cheng, and D.-H. Wei, *Phys. Rev. B* **92**, 214435 (2015).
- [16] B.-Y. Wang, M.-S. Tsai, C.-W. Huang, C.-W. Shih, C.-J. Chen, K. Lin, J.-J. Li, N.-Y. Jih, Chun-I Lu, T.-H. Chuang, and D.-H. Wei, *Phys. Rev. B* **96**, 094416 (2017).
- [17] B.-Y. Wang, C.-H. Hsiao, B.-X. Liao, C.-Y. Hsu, T.-H. Li, Y.-L. Hsu, Y.-M. Lai, M.-S. Tsai, T.-H. Chuang, and D.-H. Wei, *Phys. Rev. B* **104**, 024424 (2021).
- [18] B.-Y. Wang, J.-Y. Lee, W.-L. Li, K. Lin, M.-S. Tsai, T.-H. Chuang, and D.-H. Wei, *Phys. Rev. B* **107**, 104429 (2023).
- [19] R. K. Han, L. Liu, H. L. Sun, H. R. Qin, X. P. Zhao, D. Pan, D. H. Wei, and J. H. Zhao, *Phys. Rev. Appl.* **19**, 024033 (2023).
- [20] T. Ambrose and C. L. Chien, *Phys. Rev. Lett.* **76**, 1743 (1996).
- [21] J. Stöhr and H. C. Siegmann, *Magnetism: From Fundamentals to Nanoscale Dynamics* (Springer, New York, 2006).
- [22] N. Nakajima, T. Koide, T. Shidara, H. Miyauchi, H. Fukutani, A. Fujimori, K. Iio, T. Katayama, M. Nývlt, and Y. Suzuki, *Phys. Rev. Lett.* **81**, 5229 (1998).
- [23] M. T. Johnsony, P. J. H. Bloemenz, F. J. A. den Broeder, and J. J. de Vries, *Rep. Prog. Phys.* **59**, 1409 (1996).
- [24] T. Burkert, L. Nordström, O. Eriksson, and O. Heinonen, *Phys. Rev. Lett.* **93**, 027203 (2004).
- [25] A. Winkelmann, M. Przybylski, F. Luo, Y. Shi, and J. Barthel, *Phys. Rev. Lett.* **96**, 257205 (2006).
- [26] J. S. Kouvel and J. S. Kasper, *J. Phys. Chem. Solids* **24**, 529 (1963).
- [27] H. Umebayashi and Y. Ishikawa, *J. Phys. Soc. Jpn.* **21**, 1281 (1966).
- [28] W. Kuch, L. I. Chelaru, F. Offi, J. Wang, M. Kotsugi, and J. Kirschner, *Phys. Rev. Lett.* **92**, 017201 (2004).
- [29] M. Ekholm and I. A. Abrikosov, *Phys. Rev. B* **84**, 104423 (2011).
- [30] B.-Y. Wang, J.-Y. Ning, T.-H. Li, C.-C. Chung, C.-Y. Hsu, M.-S. Tsai, T.-H. Chuang, and D.-H. Wei, *Phys. Rev. B* **105**, 184415 (2022).
- [31] J. T. Kohlhepp and W. J. M. de Jonge, *Phys. Rev. Lett.* **96**, 237201 (2006).

- [32] J. T. Kohlhepp, H. Wieldraaijer, and W. J. M. de Jonge, *Appl. Phys. Lett.* **89**, 032507 (2006).
- [33] fcc-like Mn films have been observed to exhibit a slightly higher AFM ordering temperature than that of $\text{Fe}_{50}\text{Mn}_{50}$ films when the films are in a bulk state ($\text{Fe}_{50}\text{Mn}_{50} = 500$ K and fcc-like Mn = 540 K) [34,35].
- [34] H. Umebayashi and Y. Ishikawa, *J. Phys. Soc. Jpn.* **21**, 1614 (1966).
- [35] Y. Endoh and Y. Ishikawa, *J. Phys. Soc. Jpn.* **30**, 1614 (1971).
- [36] P. J. Hsu, Chun-I Lu, Y. H. Chu, B. Y. Wang, C. B. Wu, L. J. Chen, S. S. Wong, and M. T. Lin, *Phys. Rev. B* **85**, 174434 (2012).
- [37] C. B. Wu, J. Song, and W. Kuch, *Appl. Phys. Lett.* **101**, 012404 (2012).
- [38] Q. Li, J.-H. Liang, Y.-M. Luo, Z. Ding, T. Gu, Z. Hu, C.-Y. Hua, H.-J. Lin, T.-W. Pi, S.-P. Kang, C. Won, and Y.-Z. Wu, *Sci. Rep.* **6**, 22355 (2016).
- [39] W. C. Lin, C. C. Kuo, C. L. Chiu, and M. T. Lin, *Surf. Sci.* **478**, 9 (2001).
- [40] J. Stöhr, Y. Wu, B. D. Hermsmeier, M. G. Samant, G. R. Harp, S. Koranda, D. Dunham, and B. P. Tonner, *Science* **259**, 658 (1993).
- [41] C. M. Schneider and G. Schönense, *Rep. Prog. Phys.* **65**, 1785 (2002).
- [42] D.-H. Wei, Y.-L. Chan, and Y.-J. Hsu, *J. Electron Spectrosc. Relat. Phenom.* **185**, 429 (2012).
- [43] F. Offi, W. Kuch, and J. Kirschner, *Phys. Rev. B* **66**, 064419 (2002).
- [44] K. Lenz, S. Zander, and W. Kuch, *Phys. Rev. Lett.* **98**, 237201 (2007).
- [45] A. Scholl, J. Stöhr, J. Lüning, J. W. Seo, J. Fompeyrine, H. Siegart, J. P. Locquet, F. Nolting, S. Anders, E. E. Fullerton, M. R. Scheinfein, and H. A. Padmore, *Science* **287**, 1014 (2000).
- [46] F. Nolting, A. Scholl, J. Stöhr, J. W. Seo, J. Fompeyrine, H. Siegart, J. P. Locquet, S. Anders, J. Lüning, E. E. Fullerton, M. F. Toney, M. R. Scheinfein, and H. A. Padmore, *Nature (London)* **405**, 767 (2000).
- [47] W. Kim, E. Jin, J. Wu, J. Park, E. Arenholz, A. Scholl, C. Hwang, and Z. Q. Qiu, *Phys. Rev. B* **81**, 174416 (2010).
- [48] W. J. Antel, Jr., F. Perjeru, and G. R. Harp, *Phys. Rev. Lett.* **83**, 1439 (1999).
- [49] B.-Y. Wang, J.-Y. Hong, N.-Y. Jih, K.-H. O. Yang, L.-R. Chen, H.-J. Lin, Y.-L. Chan, D.-H. Wei, and M.-T. Lin, *Phys. Rev. B* **90**, 224424 (2014).
- [50] F. Offi, W. Kuch, L. I. Chelaru, K. Fukumoto, M. Kotsugi, and J. Kirschner, *Phys. Rev. B* **67**, 094419 (2003).
- [51] K. Binder and A. P. Young, *Rev. Mod. Phys.* **58**, 801 (1986).
- [52] Z. Q. Qiu and N. V. Smith, *J. Phys.: Condens. Matter* **14**, R169 (2002).
- [53] D. H. Wei, X. Y. Xu, L. F. Yin, G. S. Dong, and X. F. Jin, *Phys. Rev. B* **80**, 092403 (2009).
- [54] W. Kuch, X. Gao, and J. Kirschner, *Phys. Rev. B* **65**, 064406 (2002).
- [55] M. T. Lin, C. H. Ho, C. R. Chang, and Y. D. Yao, *Phys. Rev. B* **63**, 100404(R) (2001).